

Supplementary Information for Quantitative Morphological Characterization of Bicontinuous Pickering Emulsions via Interfacial Curvatures

M. Reeves, K. Stratford and J. H. J. Thijssen*

*j.h.j.thijssen@ed.ac.uk

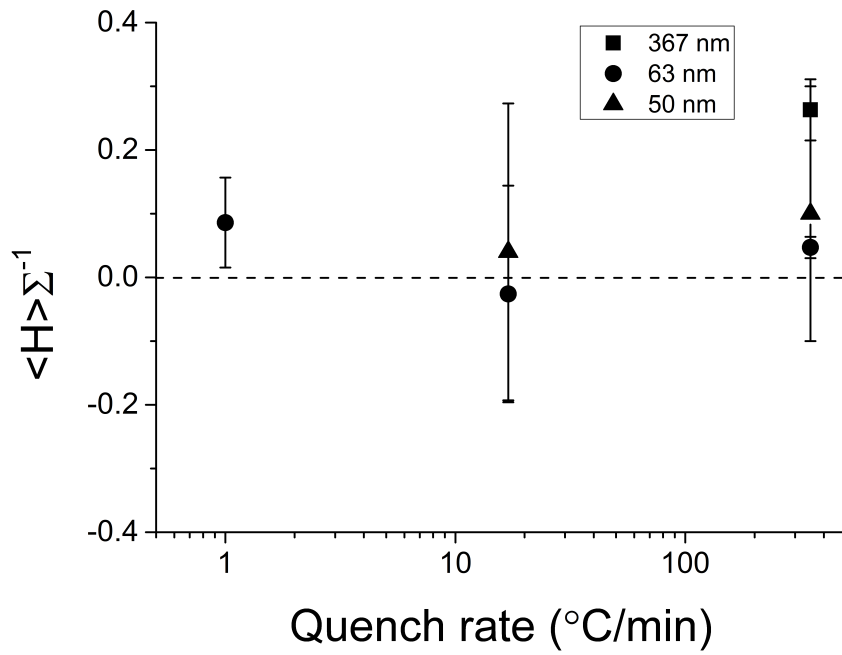
1 Errors

We have noticed that the threshold value used to create the isosurface most closely resembling the raw data (assessed by visual inspection) was the one which also maximized the area of the isosurface. For comparing curvatures across a range of samples therefore, the threshold value for the maximum area was found, and those curvature values recorded. To take account of sampling error, the entire procedure (from sample preparation, to data acquisition, to image analysis) was repeated three times, and an average of quantities taken. Where repeat sampling was not feasible (e.g. not enough identical material being available) the threshold value was varied around that which gave the maximum area, and an average of those curvature values taken. Hence, the error bars on these data points represent the thresholding error in the measurement of one sample. It is made clear in the text which data points have been multiply sampled and which have not. Also, the thresholding error was found to decrease when using a 40× objective rather than a 20× objective, but that the absolute curvature values were not affected – see Supplementary Table 1.

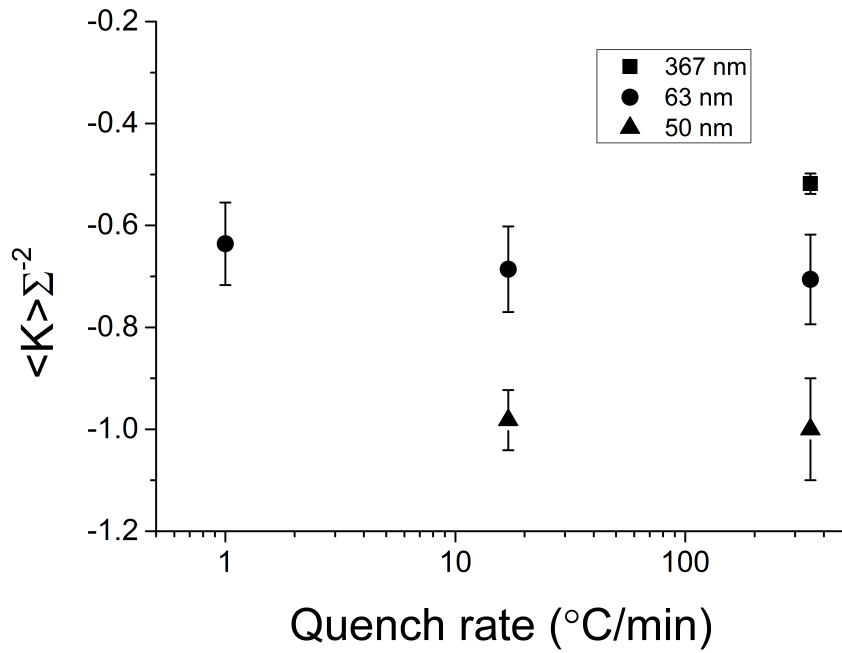
Another source of error is due to the ‘fishtank’ effect, whereby the position of the focal plane moves either more or less than the nominal Z increment depending on the relative refractive indices of the sample medium and the medium surrounding the collection optics. In this case, by using the average refractive index of the water/lutidine mixture¹ ($n_{WL} \approx 1.4$), and the refractive index of the collection medium (air, $n_A \approx 1$) the correction is calculated to be $n_{WL}/n_A = 1.4$ times the nominal Z difference.² Therefore, the analysis has also been tested on the stretched data, by modifying the voxel sizes specified when loading the data into Avizo. We found that the fishtank effect, while slightly modifying the absolute numbers, did not significantly affect the trends in the data – see Supplementary Figures 1 and 2.

Location	Magnification	$\langle K \rangle \Sigma^{-2}$	\pm
A	20×	-0.50	0.06
B	20×	-0.49	0.08
C	40×	-0.50	0.01
D	40×	-0.49	0.01

Supplementary Table 1: The results of a curvature analysis performed on a nanoparticle stabilized bijel quenched at 350°C/min, sampled at four different positions (A-D) and using two different objectives (20× and 40×). Samples showed good internal consistency, with the only effect of changing objective being a reduced thresholding error.

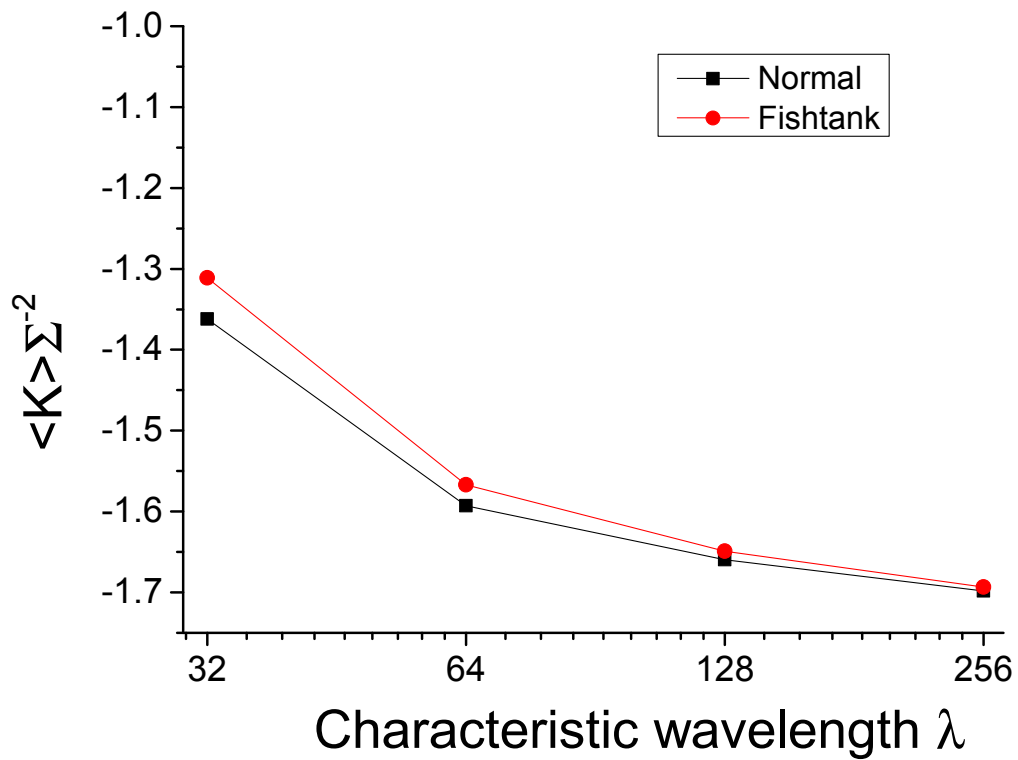


(a)



(b)

Supplementary Figure 1: The area-averaged mean curvatures (a) and Gaussian curvatures (b) as a function of quench rate, with the three sizes of particles used in the study, after the data has been corrected for the fishtank effect. The absolute values are slightly changed, but the trends remain. This analysis was not used in the main paper because of the non-linear effect of stretching the voxels on the accuracy of the curvature measurement protocol, as evidenced in Supplementary Figure 2.



Supplementary Figure 2: The area-averaged Gaussian curvature of a simulated gyroid, in a volume of 512 by 512 by 128 pixels, as a function of the gyroid wavelength (black), and the same after correcting for the fishtank effect (red). As the wavelength is reduced, the curvature measurement protocol becomes less accurate, i.e. produces a result further from the theoretical result expected (≈ -1.7). Also, the fishtank effect becomes more prominent as the wavelength is reduced. However, our data lies in the range between $\lambda=128$ and $\lambda=256$ pixels, where the curvature analysis protocol is hardly affected by taking into account the fishtank effect.

2 Temperature gradients

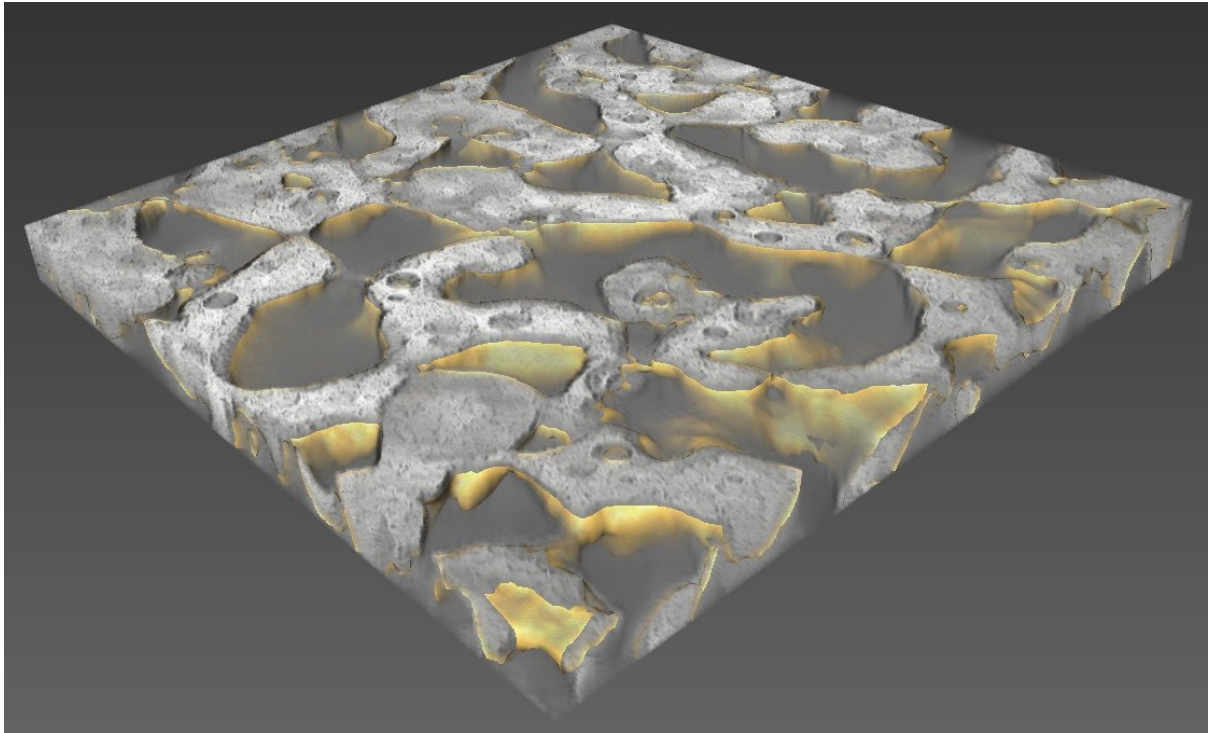
To account for the potential impact of temperature gradients, we have characterized our quenching procedures. For slow quenches, i.e. between 1 and 5°C/min, we have verified using a thermocouple that the sample temperature doesn't lag the stage temperature. For the fastest quenches (350°C/min), we use microwave heating which should heat the sample homogeneously. For the medium quench rate of 17°C/min, there could be significant temperature gradients in the sample cell, but they are minimized by encasing the cell completely in an aluminium block. In previous studies these gradients result in the confocal microscopy images showing one part of the sample at a later stage of spinodal decomposition than another part.³ In the present study we have not seen this – confocal microscopy timeseries of the phase separation show homogenous phase separation, as in Reeves *et al.*⁴ (we use the same preparation method here). Also in Reeves *et al.* the samples were scanned to analyze homogeneity and no significant variation in structure was found, implying non-significant temperature gradients.⁴

3 Sample specifications

Radius (nm)	Vol. frac. (%)	Quench rate (°C/min)
367	2.8	350
367	2.8	350
367	2.8	350
63	0.7	350
63	0.7	350
63	1.0	350
50	1.4	350
63	0.6	17
63	1.0	17
63	2.3	17
50	1.4	17
63	1.8	1

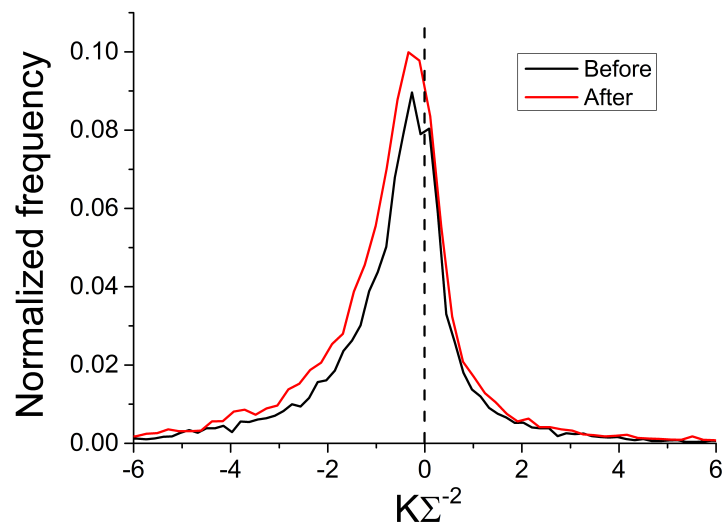
Supplementary Table 2: The specifications of bijel samples prepared for subsequent characterization and comparison in this paper. The parameter space is such that we can look for the effect of particle size and quench rate on the bijel's curvature distributions (see main text). Note that in some cases where we fix the particle size and vary quench rate, the volume fraction is not fixed. The effect of changing the volume fraction is to change the final bijel lengthscale L via $L \propto r/\phi$ which also changes the range of interfacial curvature values. However, we account for this by normalizing the curvature values with respect to the surface to volume ratio. We also average the results from multiple samples (where possible) to show that the volume fraction does not play a pivotal role in determining the topology of the final structure (see main paper section 2.5).

4 Isosurface accuracy



Supplementary Figure 3: A 3D volume rendering of a microparticle stabilized bijel (greyscale) with the calculated isosurface superimposed (yellow). The isosurface clearly follows the pattern of the raw data, meaning that the curvature analysis performed on the isosurface can be said to represent the curvature values of the raw data, i.e. the bijel.

5 Polymerization



Supplementary Figure 4: The distributions of Gaussian curvature as measured by confocal microscopy and image analysis for a bijel just before (black) and just after (red) polymerization, induced by UV irradiation. In order to minimize scattering, we (partially) matched the polymer refractive index using Dow Corning Fluid 550. The area averaged values are $-0.69(17)$ and $-0.60(19)$ i.e. relatively similar, meaning that the polymerization process itself leaves the structure largely unchanged. Note that these values cannot be compared to the results of the main paper for MP stabilized bijels as a slightly different protocol was used here to account for a larger ratio between the size of the channels and the data volume.

6 Simulation parameters

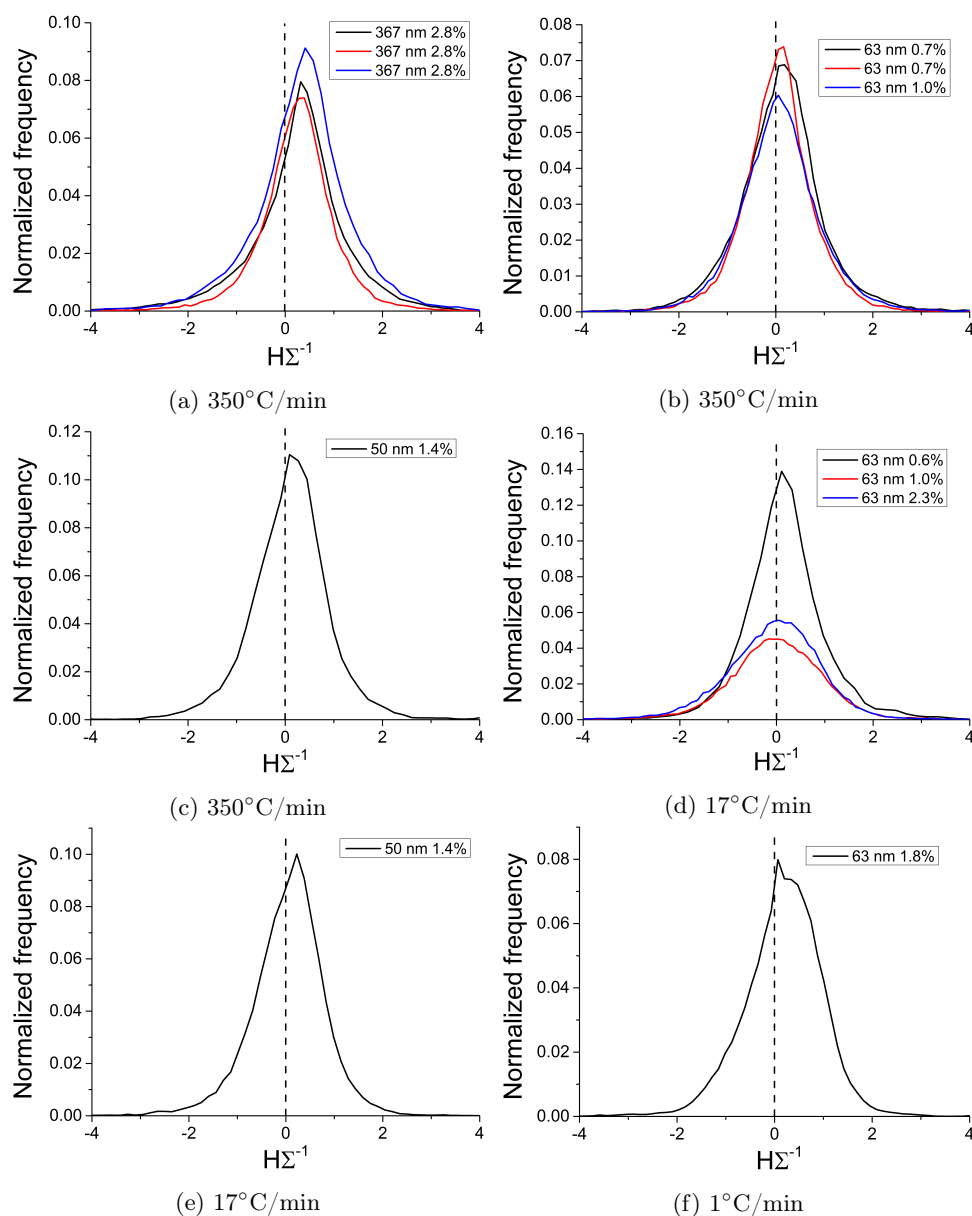
We employ a symmetric free energy (e.g., Kendon *et al.*[?]) with density as a function of composition ϕ is

$$\frac{1}{2}A\phi^2 + \frac{1}{4}B\phi^4 + \frac{1}{2}\kappa(\nabla\phi)^2. \quad (1)$$

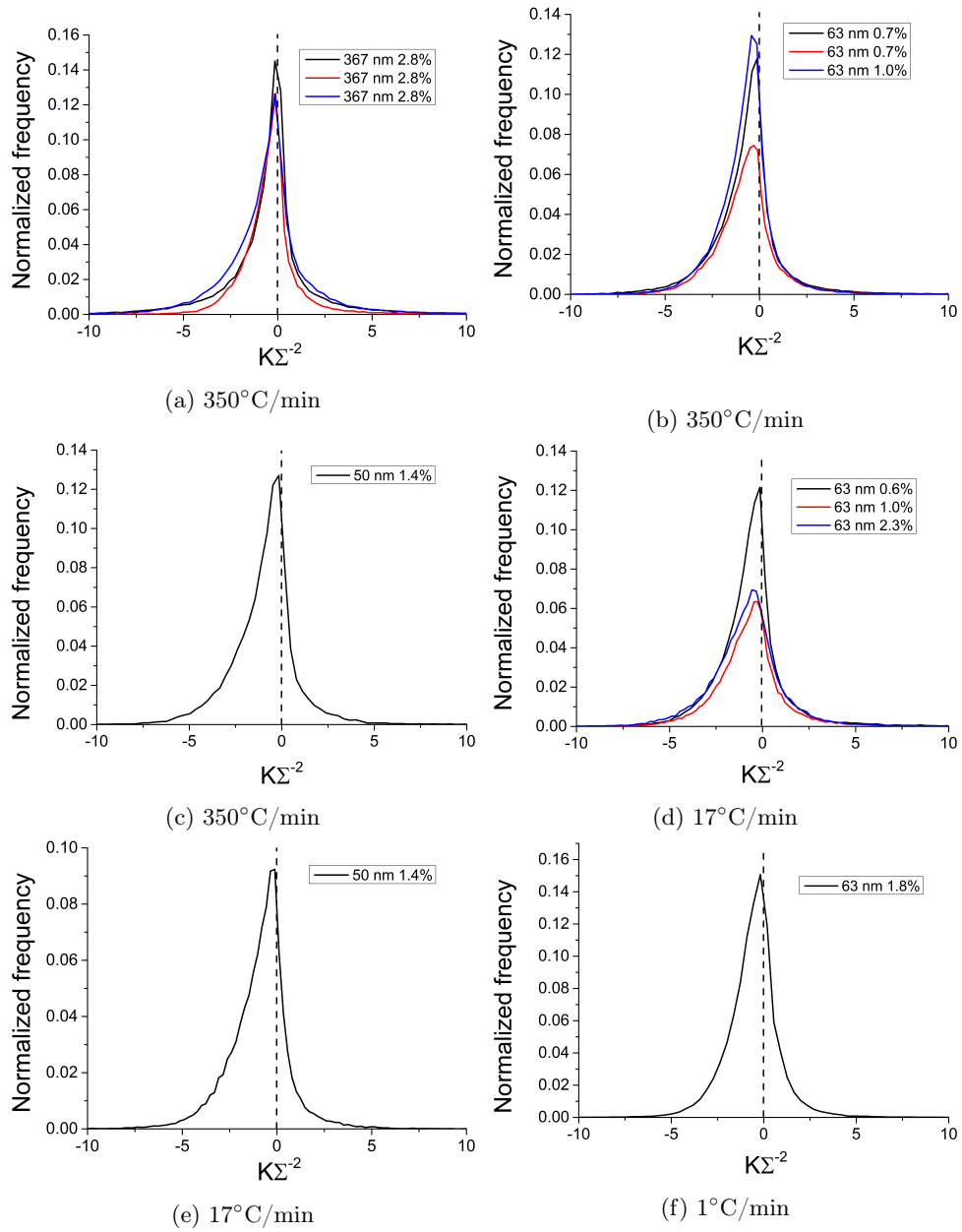
The parameters A , B , and κ control the fluid-fluid interfacial tension, and also the interfacial thickness. We choose the parameters $A = -B = -0.00025$ and $\kappa = 0.000175$ giving an interfacial tension of $\sigma \approx 1.97 \times 10^{-4}$ in simulation units. The interfacial width is 1.18 simulation units. Fluid parameters were density $\rho = 1$ and dynamic viscosity $\eta = 0.12$. Neutrally wetting (contact angle 90°) spherical particles with radius $a = 2.3$ lattice units were used. Fluctuating hydrodynamics is used to impart Brownian motion to the particles with effective temperature 2.12×10^{-6} in simulation units. A system size of $256 \times 256 \times 128$ lattice units was used, in which the fluid volume ratio was initialized to 65 : 35 by volume before particles were inserted randomly in the initial condition (32,919 colloids). Spinodal decomposition was initiated via a small-amplitude random noise in the order parameter ϕ .

The simulation parameters – in ‘simulation units’ – may be matched with the experimental parameters as follows. We assume a simplified experiment with fluids of uniform density $1.0 \times 10^3 \text{ kg}\cdot\text{m}^{-3}$, and viscosity $1.0 \times 10^{-3} \text{ Pa}\cdot\text{s}$, and with an interfacial tension $5.0 \times 10^{-4} \text{ N}\cdot\text{m}^{-1}$. The characteristic length and time scales for spinodal decomposition are $L_0 = \eta^2/\rho\sigma$ and $T_0 = \eta^3/\rho\sigma^2$. By matching these quantities in experiment and simulation we may equate 1 simulation length unit to 23 nm (a particle radius of 63 nm and system size of 3 μm in the short direction), and 1 simulation time unit to $9 \times 10^{-11} \text{ s}$. Temperature is matched via a dimensionless diffusion constant $6\pi DT_0/L_0^2$: the simulation temperature corresponds to approximately 300 K.

7 Curvature distributions

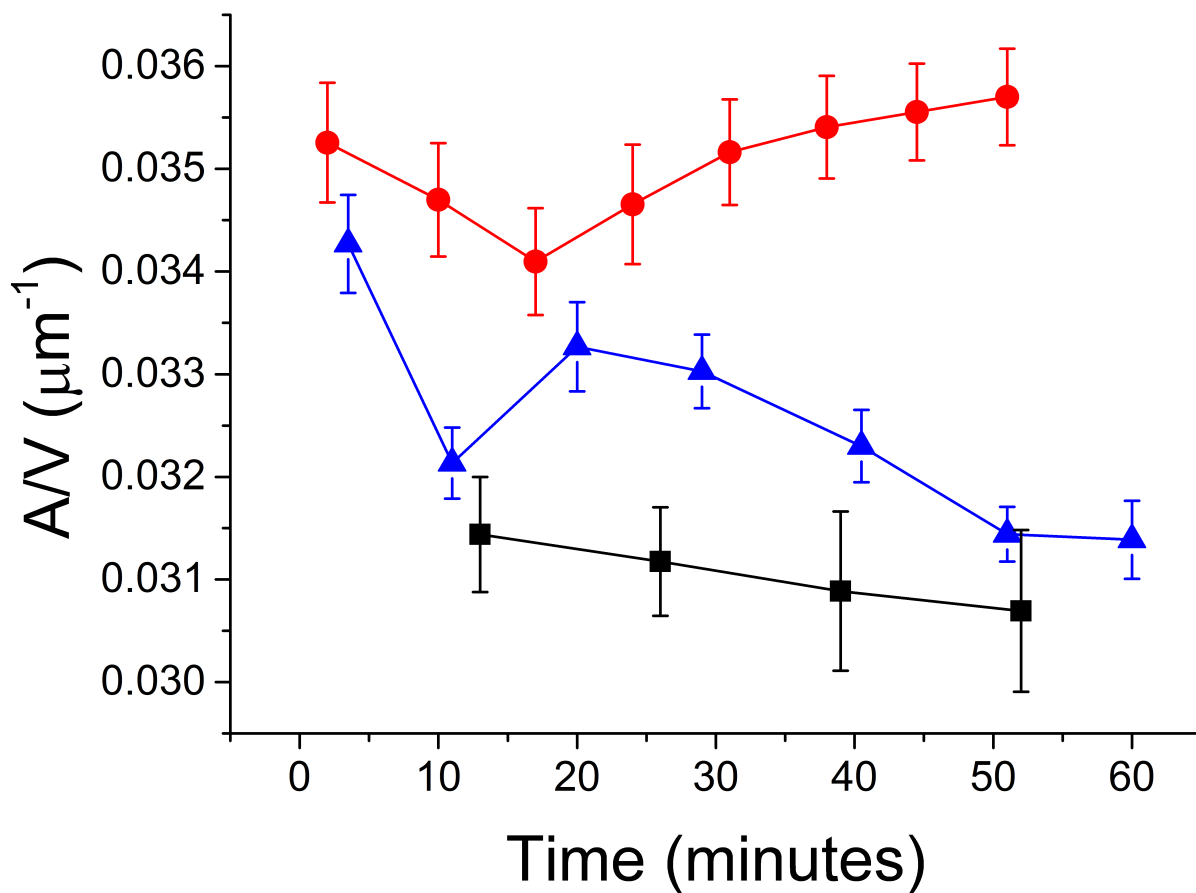


Supplementary Figure 5: The normalized frequency distributions of mean curvatures $H\Sigma^{-1}$ for the samples studied in Figures 7 & 8 of the main paper and explicitly outlined in sections 3.2 and 3.3. All of the distributions are within one half-width at half-maximum of zero suggesting a non-significant departure from zero.



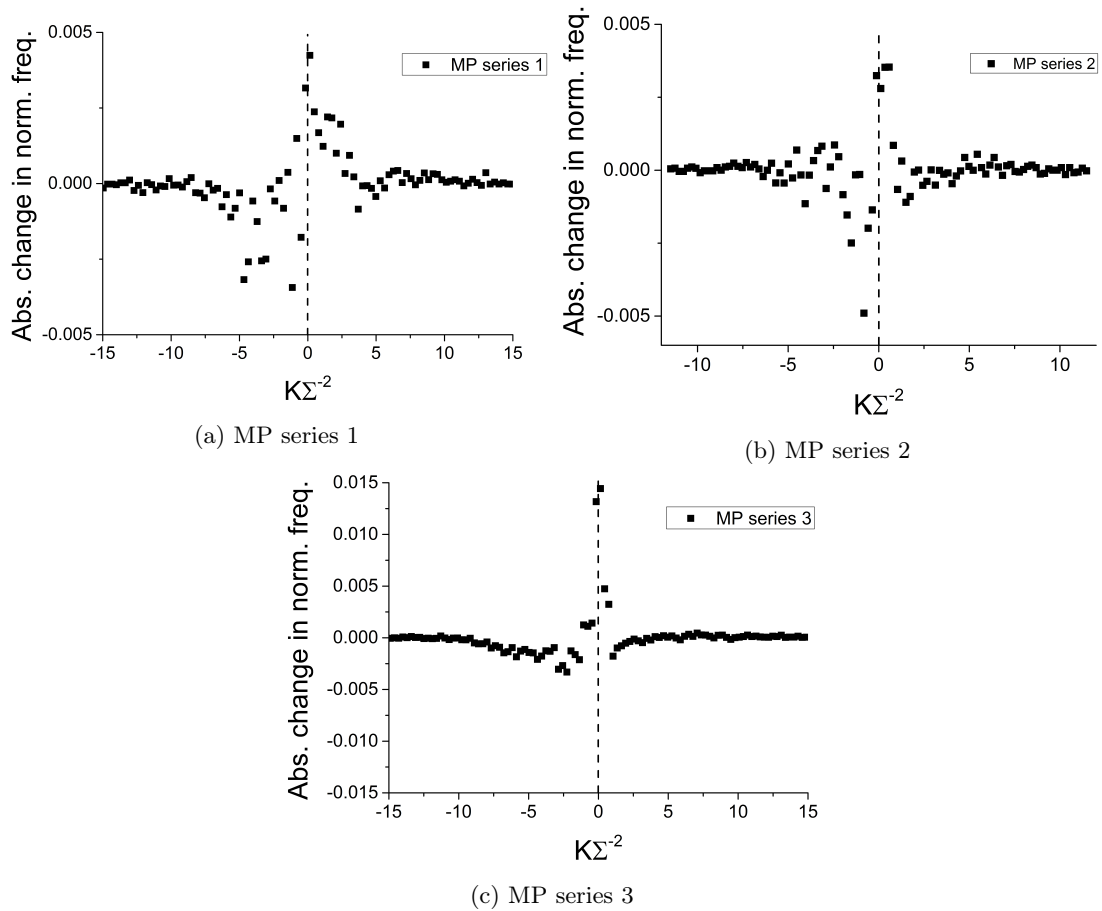
Supplementary Figure 6: The normalized frequency distributions of Gaussian curvatures $K\Sigma^{-2}$ for the samples studied in Figures 7 & 8 of the main paper and explicitly outlined in sections 3.2 and 3.3. All of the distributions are within one half-width at half-maximum of zero suggesting a non-significant departure from zero.

8 Surface to volume ratios



Supplementary Figure 7: The change in the surface-to-volume ratio (A/V) as a function of time from the onset of phase separation, in the case of three separately prepared microparticle-stabilized bijels: the same ones as presented in Figure 9(a) of the main text. A reduction in A/V indicates coarsening of the bicontinuous structure – this is observed in 2 out of 3 of the data sets. The behaviour of the red data set can be accounted for by a slight drift in the bijel sample relative to the data volume, meaning that this data set is a less reliable measure of any time dependence in A/V . Nonetheless, any change in area-averaged curvature cannot be explained by coarsening, since the curvatures are normalized with respect to A/V .

9 Change in distributions over time



Supplementary Figure 8: The absolute change in the area-averaged Gaussian curvature distributions between the first and last time point in the three timeseries presented in Figure 9(a) of the main paper. The largest changes take place around the $K\Sigma^{-2} = 0$ line, implying that points of small negative Gaussian curvature mutate into points of small positive Gaussian curvature.

References

- [1] C. A. Grattoni, R. A. Dawe, C. Y. Seah and J. D. Gray, *J. Chem. Eng. Data*, 1993, **38**, 516–519.
- [2] <https://svi.nl/FishtankEffect>, accessed on 26th October 2015.
- [3] K. A. White, A. B. Schofield, B. P. Binks and P. S. Clegg, *J. Phys.: Condens. Matter*, 2008, **20**, 494223.
- [4] M. Reeves, A. T. Brown, A. B. Schofield, M. E. Cates and J. H. J. Thijssen, *Phys. Rev. E.*, 2015, **92**, 032308.